Tropospheric haze and colors of the clear daytime sky

Raymond L. Lee, Jr.

Mathematics and Science Division, United States Naval Academy, Annapolis, Maryland 21402, USA (raylee@usna.edu)

Received 11 August 2014; accepted 24 November 2014;
posted 15 December 2014 (Doc. ID 220709); published 23 January 2015

To casual observers, haze's visible effects on clear daytime skies may seem mundane: significant scattering by tropospheric aerosols visibly (1) reduces the luminance contrast of distant objects and (2) desaturates sky blueness. However, few published measurements of hazy-sky spectra and chromaticities exist to compare with these naked-eye observations. Hyperspectral imaging along sky meridians of clear and hazy skies at one inland and two coastal sites shows that they have characteristic colorimetric signatures of scattering and absorption by haze aerosols. In addition, a simple spectral transfer function and a second-order scattering model of skylight reveal the net spectral and colorimetric effects of haze.

OCIS codes: (010.1290) Atmospheric optics; (010.1310) Atmospheric scattering; (010.1690) Color; (010.3920) Meteorology; (290.1090) Aerosol and cloud effects; (330.1730) Colorimetry.
http://dx.doi.org/10.1364/AO.54.00B232

1. Introduction

For students of atmospheric radiative transfer, tropospheric haze has long been a source of highly valuable, if often difficult, lessons on spectral scattering and extinction [1–5]. Yet on the subject of clear-sky colors, haze may at first seem to have little to teach us. After all, does not scattering by haze droplets merely (1) reduce distant objects' luminance contrast and (2) desaturate sky blueness? Although the answer to both questions is a qualified "yes" [6,7], this answer's details have been explored only occasionally [8–13]. Many such studies of haze's effects on skylight spectra and colors are often restricted to near-horizon paths (*i.e.*, to directions with view-elevation angle $h \sim 0°$) [8,11,14–16]. Furthermore, some authors are interested in object colors seen over long optical pathlengths, rather than skylight colors *per se* [13,17]. This limits the lessons on haze colors that can be drawn from such studies.

To define this color palette more fully, both a spectroradiometer [18] and a hyperspectral imaging system [19] were used to measure narrow field-of-view (FOV) skylight along sky meridians (*i.e.*, at constant azimuth relative to the sun ϕ_{rel}) in 20 clear daytime skies from 2010 to 2013. Although unrefracted sun elevations h_0 ranged from 3° to 45° for these meridional scans, most were made when $h_0 \sim 30°$ so that at shared azimuths of $\phi_{\mathrm{rel}} = 90°$, 180°, and 270° their single-scattering angles Ψ are comparable. The resulting skylight spectra and chromaticities come from both coastal and inland sites, and they consistently show *visible* spectral shifts associated with changes in aerosol normal optical depth τ_{aer}. Although the chromaticity patterns are similar to those obtained from colorimetrically calibrated digital photographs [10,20], such three-channel techniques have metameric uncertainties that are avoided by calculating chromaticities from detailed spectra.

An important caveat applies to the spectral and colorimetric results presented here. As both Henry *et al.* [11] and Lynch and Mazuk [13] note, even spectrally calculated chromaticities may not predict color appearance realistically. Thus an outdoor observer's visual perception of sky color is only indirectly related to absolute chromaticity. Among other factors, viewing duration and observer FOV, luminance level, and simultaneous color contrast can all affect a person's direct visual experience of skylight.

1559-128X/15/04B232-09$15.00/0

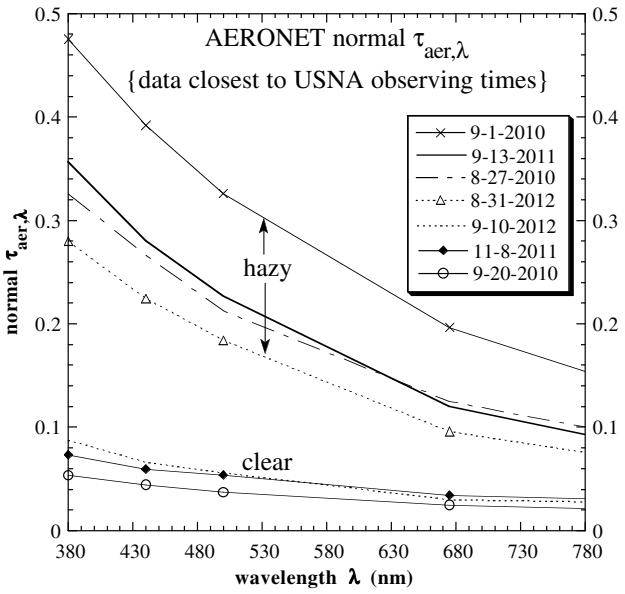

Fig. 1. Aerosol normal optical depths for extinction $\tau_{\mathrm{aer},\lambda}$ measured at AERONET sun photometer sites near the United States Naval Academy (USNA) in Annapolis, Maryland at times closest to this paper's measured skylight spectra.

However, persistent chromaticity trends that occur over wide FOVs are more likely to correspond to perceptible skylight features. One common example is the decrease in sky blueness near the horizon, a trend that is both measurable and readily seen. So the emphasis here is on skylight color and spectral *trends*, rather than on absolute chromaticities.

2. Measured Chromaticities of Clear and Hazy Skies at USNA

Most of the clear-sky spectra in this paper were measured at the United States Naval Academy (USNA) in Annapolis, Maryland, which is located on the Chesapeake Bay's western shore at 38.983° N, 76.484° W. Additional measurements were made at a rural inland site near Marion Center, Pennsylvania at 40.810° N, 79.080° W (elevation above mean sea level = 451 m) and at the summit of Cadillac Mountain, Maine at 44.353° N, 68.224° W (elevation = 470 m) near the Atlantic Ocean. Figure 1 plots the spectral aerosol extinction $\tau_{\mathrm{aer},\lambda}$ measured near USNA in several clear and hazy skies as a function of wavelength λ [21]. Although optical depth data is not available for the other two sites, Table 1 lists their meteorological ranges V' as well as USNA's 380-nm $\tau_{\mathrm{aer},\lambda}$. For all sites, the visual criterion for the presence of tropospheric haze (as opposed to stratospheric haze) is that the contrast of distant objects near the horizon must be perceptibly less than under the least turbid conditions.

Haze aerosols at coastal sites such as USNA and Cadillac Mountain typically are solution droplets that form by deliquescence and have modal diameters of ~0.1 μm [22,23], and both locations' aerosol species tend to be dominated by dissolved sulfates [24]. A further distinction is sometimes made between dry haze and damp haze, with the latter being caused by scatterers of diameter >0.1 μm [25]. If the slant-path aerosol optical thickness τ_{slant} through a haze layer is relatively small (say, $\tau_{\mathrm{slant}} < 0.3$), then spectrally selective scattering by the smaller particles of dry haze will make it appear bluish when seen against a dark background. Conversely, spectrally neutral scattering by the larger particles in damp haze can be expected to make it appear white or grayish for any τ_{slant} [26,27].

Some of these haze properties are evident in Fig. 2, which pairs a clear, haze-free sky in Fig. 2(a) with a visually hazy one in Fig. 2(b). Because of their similar h_0 and scattering symmetry about the clear-sky principal plane (*i.e.*, $\phi_{\mathrm{rel}} = 90°$ and 270° produce identical single-scattering results), these visible-wavelength color images span the same range of single-scattering Ψ. Both images are calculated from meridional hyperspectral scans made with the Resonon Pika II imaging spectrometer [19]. Each scan required ~16 sec to complete, and each has angular dimensions of ~45° by 36°. Because trees at the bottom of Fig. 2(b) are only ~1 km away, their contrast against the horizon sky is reduced only slightly compared with trees seen through Fig. 2(a)'s less turbid atmosphere [28]. However, some more obvious visual signs of the much larger $\tau_{\mathrm{aer},\lambda}$ in Fig. 2(b) are its: (1) broader local maximum in sky luminance L_v near the horizon, (2) more desaturated sky colors there,

Table 1. Geometrical and Colorimetric Parameters for Haze-related Color Changes in Figs. 1–12

Figure(s)	Date (month-day-year)	site name	h-interval for $\hat{g}$ (°)	ϕ_{rel} (°)	mean u'	mean v'	$\hat{g}$	h_0 (°)	$\tau_{\mathrm{aer},\lambda}$ at 380 nm
1, 4	9-1-2010	USNA	1.5–46	270	0.18621	0.45248	0.039692	30.2	0.4752
1, 2(b), 3, 5, 11(a), 12	9-13-2011	USNA	1.5–46	270	0.18586	0.44252	0.041353	33.4	0.3568
1, 5	8-27-2010	USNA	2.4–47	180	0.17882	0.43333	0.046378	42.9	0.3257
1, 9, 10	8-31-2012	USNA	n/a	90, 180	n/a	n/a	n/a	30	0.2799, 0.08727
1, 4	11-8-2011	USNA	0.7–45	270	0.17883	0.4217	0.048756	32.6	0.07341
1, 2(a), 3, 7	9-20-2011	USNA	1.1–46	90	0.17632	0.43031	0.051016	30.4	0.05346
8	8-1-2013	Cadillac	1.2–90	93	0.17741	0.41509	0.033822	39.2	($V' \sim 15$ km)
8	8-1-2013	Cadillac	0.6–90	180	0.17622	0.40925	0.044723	41.0	($V' \sim 15$ km)
6(a), 7	10-9-2011	Marion Center	2.0–46	90	0.18162	0.43066	0.048275	30.6	($V' > 30$ km)

Note: Rows are sorted in order of decreasing normal optical depth $\tau_{\mathrm{aer},\lambda}$ at 380 nm.

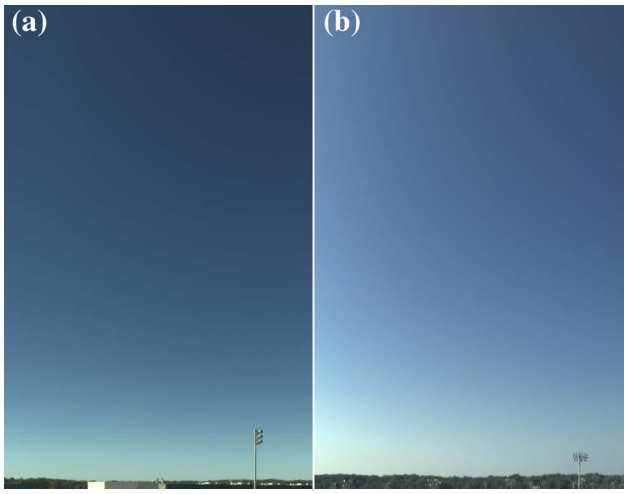

Fig. 2. Visible-wavelength images calculated from hyperspectral scans made along fixed sky meridians for view-elevations $h \sim 0°$–$46°$ at USNA on the (a) haze-free day of 20 September 2010 at unrefracted sun elevation $h_0 = 30.4°$ and relative azimuth $\phi_{rel} \sim 90°$, and (b) hazy day of 13 September 2011 at $h_0 = 33.4°$ and $\phi_{rel} \sim 270°$ at image center. For display purposes, the latter scan is flipped horizontally so that the sun is to the left of both images.

and (3) greater dynamic range in L_v along almucantars (note especially the stronger brightening near Fig. 2(b)'s left or sunward edge).

Figure 3 plots the distinct colorimetric differences between Figs. 2(a) and 2(b) in a section of the CIE 1976 uniform-chromaticity-scale (UCS) diagram. Colorimetric landmarks in Fig. 3 include part of the Planckian or blackbody locus and its corresponding color-temperature limits, with bluer (*i.e.*, higher color temperature) colors to the lower left and redder colors (*i.e.*, lower color temperatures) to the upper right. To provide a perceptual scale here and in subsequent UCS diagrams, the major semiaxis of a

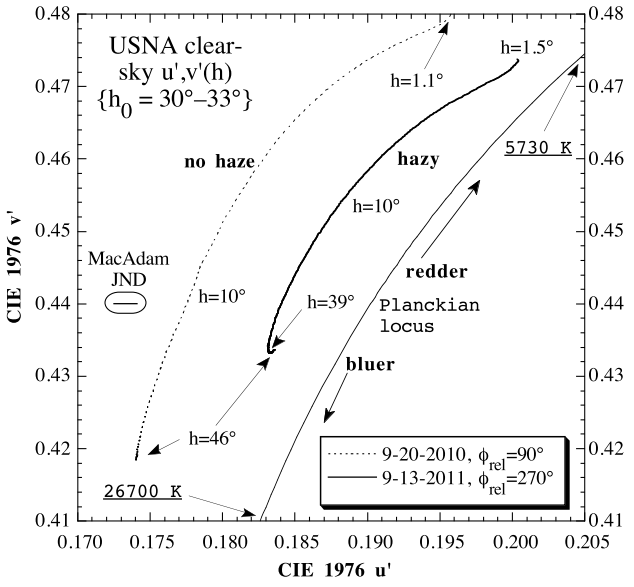

Fig. 3. Meridional u', $v'(h)$ chromaticity curves measured for Fig. 2's clear and hazy skies, with each plotted u', v' chromaticity coordinate averaged at constant h across an interval $\Delta\phi_{rel} = 4°$. See Table 1 for additional colorimetric and geometrical details.

local MacAdam just-noticeable difference (JND) is drawn near Fig. 3's left ordinate [29]. Separate meridional chromaticity curves of u', $v'(h)$ are drawn in Fig. 3 for Fig. 2's clear and hazy skies.

In Fig. 3 and other UCS diagrams, u', v' chromaticity coordinates are averaged at constant h across an interval $\Delta\phi_{rel} = 4°$ wide (sample size $N = 88$ hyperspectral pixels per u', v' pair). The lowest h of each scan was measured with a calibrated digital inclinometer (repeatability of $\pm 0.1°$), and higher h were calculated as the cumulative angular width of subsequent scan lines. ϕ_{rel} was set with a combination of (1) a sunlit gnomon aligned with the spectrometer's optical axis and (2) the true compass azimuths of surface features visible along the horizon of a scan.

Both of Fig. 3's chromaticity curves have features that correspond to our *in situ* perception of sky color. First, each of its u', $v'(h)$ curves has redder colors at lower h. In purely visual terms, this describes the everyday experience that sky colors look less blue closer to the horizon. Second, the shape of each curve is roughly that of the nearby Planckian locus. In hindsight, this near-congruence is unsurprising because clear-sky colors derive from scattered sunlight. Thus at a given time and place, meridional trends in atmospheric spectral extinction usually differ only by degree (*i.e.*, τ_{slant} changes continuously in h) rather than in kind (*i.e.*, normal $\tau_{aer,\lambda}$ spectra change very little in h). As a result, a particular daytime clear sky's meridional pattern of chromaticities tends to follow a path along the Planckian locus rather than toward or away from it.

Yet Fig. 3's chromaticity curves are dissimilar in important ways. First, its u', $v'(h)$ curve for 13 September 2011 is much closer to the Planckian locus, meaning that chromaticities for Fig. 2(b)'s hazy sky are less chromatic than those for Fig. 2(a)'s haze-free sky. However, this simple measure of clear-sky color's desaturation by haze is not infallible (see Section 3). Second, Fig. 3's shorter u', $v'(h)$ curve for 13 September 2011 shows the reduced gamut of blues in Fig. 2(b)'s hazy sky. In colorimetric terms, this particular hazy sky has a normalized colorimetric gamut $\hat{g} \sim 19\%$ smaller than that measured on 20 September 2010. (Ref. [10] defines $\hat{g}$.) Although this haze-induced gamut reduction is not negligible, it differs greatly from the colorimetric uniformity of fog. Table 1 lists Fig. 3's values for $\hat{g}$ and their corresponding mean u' and v', as well as the geometrical parameters of h_0, ϕ_{rel}, and h. Finally, Fig. 3 includes what seems at first glance to be only a minor colorimetric curiosity: a small hook in the 13 September 2011 u', $v'(h)$ curve at $h = 39°$. Yet as shown below, this seemingly small detail offers an unexpected insight into how aerosols alter clear-sky scattering. Romero *et al.* produced similar chromaticity hooks (although with opposite curvature) in their airlight simulations as horizontal distances increased between targets and observers [17].

Figure 4 shows a common variation on Fig. 3's clear-versus-hazy sky meridional chromaticity

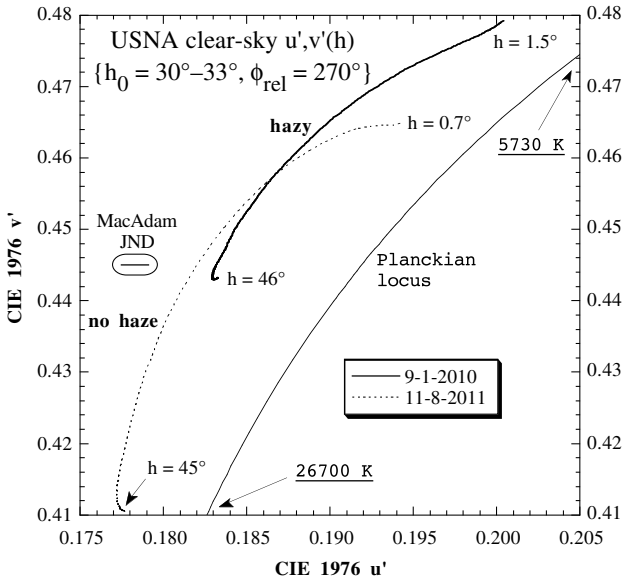

Fig. 4. Meridional CIE 1976 u', $v'(h)$ chromaticity curves measured for two different USNA clear (8 November 2011) and hazy (1 September 2010) skies at $\phi_{rel} = 270°$, with each plotted u', v' averaged at constant h across $\Delta\phi_{rel} = 4°$.

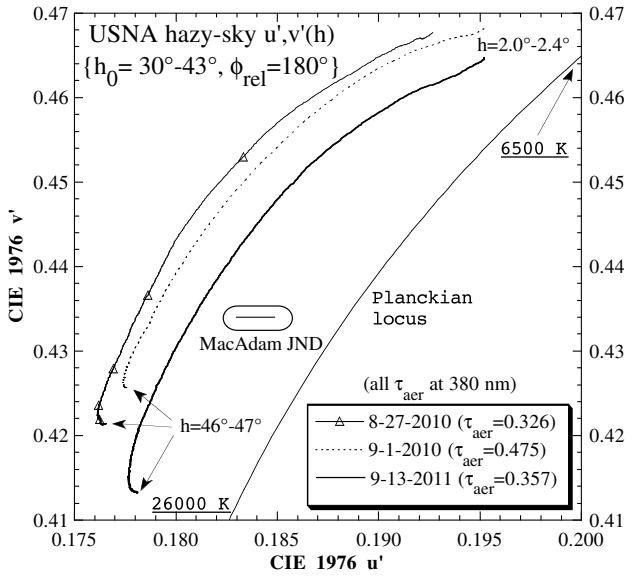

Fig. 5. Meridional u', $v'(h)$ chromaticity curves measured for three different USNA hazy skies at $\phi_{rel} = 180°$, with each plotted u', v' averaged at constant h across $\Delta\phi_{rel} = 4°$.

curves, with Table 1 again listing the corresponding colorimetric and geometrical data. Now the two curves for the hazy (1 September 2010) and clear sky (8 November 2011) are at approximately the *same* distance from the Planckian locus, although their color-temperature overlap is much less than in Fig. 3. In fact, u', $v'(h)$ curves for haze-free skies occur at fairly consistent distances from this locus, with significant green-to-purple shifts restricted to hazy skies (*i.e.*, shifts from upper left to lower right, perpendicular to the Planckian locus).

Although the cause of individual green-to-purple chromaticity shifts remains unclear, their fundamental cause is not: spectral extinction by tropospheric aerosols produces visible departures from the spectra and colors of the molecular atmosphere. As $\tau_{aer,\lambda}$ values increase across the visible spectrum, tropospheric aerosols shift scattered skylight farther away from the near-constant patterns of a purely molecular atmosphere. With greater aerosol scattering and absorption, greater spectral variety can be expected in the resulting skylight. Figure 5 shows some of this variety in three of the haziest skies measured at USNA (*i.e.*, those with the largest $\tau_{aer,\lambda}$). Across the same h interval, perceptible green-purple shifts occur in the u', $v'(h)$ curves. Yet τ_{aer} magnitudes alone do not explain these, since the meridional chromaticity curve for the highest aerosol amount (1 September 2010) is located *between* those with smaller τ_{aer}. Other spectral scans suggest that Fig. 5's fairly small differences in h_0 do not explain its colorimetric shifts.

3. Measured Chromaticities of Clear and Hazy Skies at Other Sites

Some subtle differences are visible between the hyperspectral scans in Figs. 2 and 6, with the latter coming from the rural Marion Center site on 9 October 2011. All of the color maps in Figs. 2 and 6 are calculated using exactly the same spectral integration and coordinate transform that map from the absolute spectral radiances L_λ of the Pika II to u', v' chromaticities to red-green-blue (RGB) pixel triplets. (See Ref. [29], pp. 156–159 for details of similar CIE 1931 x, y colorimetric calculations.) Even though your display device likely differs from mine in its chromaticity and luminance gamut, the pixel RGB values in Figs. 2 and 6 were produced by a single mapping algorithm. As a result, we can compare *relative* shifts in the two figures' colors, even if your color shifts differ visibly from mine.

With this important caveat in mind, note that Fig. 6(a)'s blues *look* slightly more vivid than those

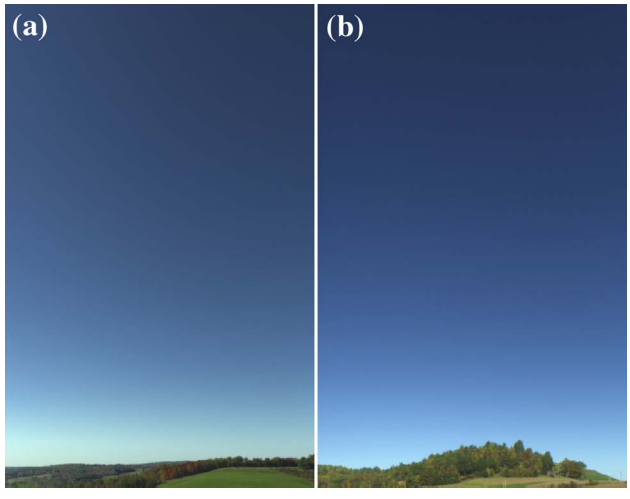

Fig. 6. Images calculated from meridional hyperspectral scans for $h \sim 0°$–$46°$ at a rural site near Marion Center, Pennsylvania on the haze-free day of 9 October 2011 for (a) $h_0 = 30.6°$, $\phi_{rel} = 90°$ and (b) $h_0 = 34.8°$, $\phi_{rel} \sim 180°$ at image center.

in Fig. 2(a), even though both scans were made using nearly identical h_0, ϕ_{rel}, and h intervals (see Table 1). Note too that the meridional range of L_v is visibly larger in Fig. 6(a), which is consistent with its having slightly purer blues [10]. Although no τ_{aer} measurements are available to supplement Fig. 6's estimated 30-km meteorological range, we can compare surface relative humidities at the two sites. Each suggests a low-turbidity troposphere: 25% on 20 September 2010 at USNA and 37% on 9 October 2011 at Marion Center.

What then might explain the two figures' visible color differences? Two possible aerosol explanations are differences in the sites' (1) elevations (20 m versus 451 m) and (2) inventory of aerosol species. However, the greatest puzzle posed by Figs. 2(a) and 6(a) is visual rather than micrometeorological. Figure 7 plots u', $v'(h)$ curves for these two figures, whose colors would differ visibly if we could compare them *in situ* as well as photographically. Despite the fact that blues look purer throughout Fig. 6(a), Fig. 7 shows that its $h = 2°$–$46°$ chromaticity curve is much *closer* to the Planckian locus, and thus the colors of Fig. 6(a) should appear closer to neutral (*i.e.*, less chromatic) than those in Fig. 2(a). Yet the opposite is true. This visual fact is all the more puzzling considering that Fig. 2(a)'s sky looks more vivid than its Fig. 2(b) counterpart, and Fig. 3 shows that Fig. 2(a)'s more vivid blues produce, as expected, a $u', v'(h)$ curve that is *farther* from the Planckian locus. Thus Fig. 6 is one case where color appearance seems at odds with colorimetry, a possibility raised in Section 1.

Despite their differences, Figs. 3–5 and 7 all share one colorimetric feature. Each UCS diagram has at least one $u', v'(h)$ curve with a small but distinct chromaticity hook near $h = 45°$. The presence of this hook seems to be independent of both τ_{aer} and absolute chromaticity. Initially, such routine reversals in clear-sky u', $v'(h)$ trends seem counterintuitive. Explaining the desaturation of skylight with decreasing h is straightforward: τ_{slant} and thus multiple scattering increase with decreasing h, with the result that skylight is redder at lower h (in the sense of being more spectrally uniform) [26,30]. But why might skylight redden slightly as h increases and τ_{slant} decreases above ~45°?

To answer this question, we start by noting the basic colorimetric features of Fig. 8 from Cadillac Mountain. First, Fig. 8's high-h chromaticity hooks are more pronounced because its meridional scans extend to the zenith, with each scan requiring ~33 sec to complete. Its two clear-sky $u', v'(h)$ curves were measured within 10 min of each other in a clear sky that had some visible haze (horizontal V'~ 15 km), a narrow band of thin cirrus near the horizon, and a few small cumulus far above it. Neither Fig. 8 scan includes these cumulus clouds, and the cirrus appear colorimetrically only as bending of the $\phi_{rel} = 180°$ curve below $h \sim 4°$. Second, the $\phi_{rel} = 93°$ and 180°curves would intersect at the single chromaticity of the zenith if these two scans were made simultaneously; their small difference in h_0 causes the curves not to intersect.

Third, to show more colorimetric detail, Fig. 8 has a smaller u' scale than do Figs. 3–5 and 7, and this by itself slightly increases the chromaticity hooks' apparent sizes. Nonetheless, including chromaticities from $h > 45°$ does in fact increase their absolute colorimetric size. Fourth, skylight is visibly bluer from Cadillac Mountain's summit at all h because of the site's slightly smaller normal τ_{aer} compared with that at sea level. Fifth, note that Fig. 8 illustrates another common property of clear skylight: compared with

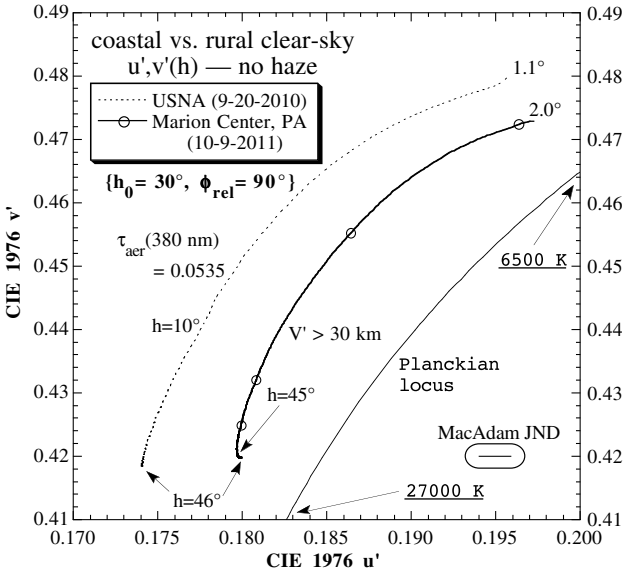

Fig. 7. Meridional $u', v'(h)$ chromaticity curves of two clear skies measured at USNA (20 September 2010) and Marion Center, Pennsylvania (9 October 2011) at $\phi_{rel} = 90°$, with each plotted u', v' averaged at constant h across $\Delta\phi_{rel} = 4°$.

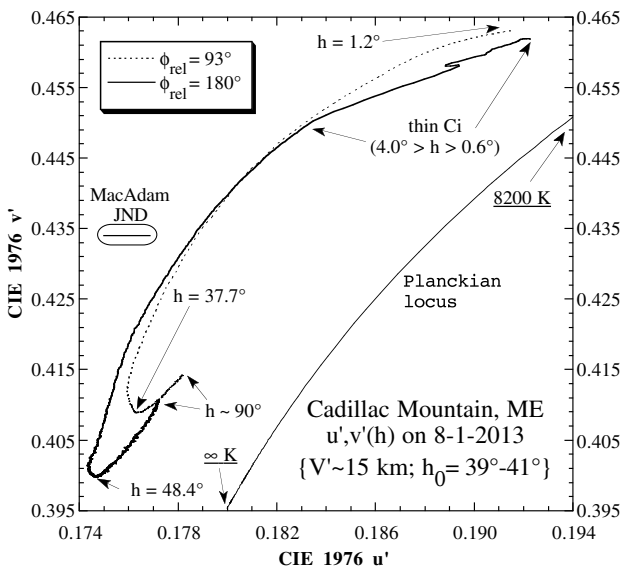

Fig. 8. Meridional $u', v'(h)$ chromaticity curves of the same slightly hazy sky measured on 1 August 2013 from the summit of Cadillac Mountain, Maine at $\phi_{rel} = 93°$ and 180°, with each plotted u', v' averaged at constant h across $\Delta\phi_{rel} = 4°$.

sky colors at right angles to the sun ($\phi_{rel} = 90°$ or 270°), colors along the antisolar azimuth ($\phi_{rel} = 180°$) of the same sky usually are bluer at corresponding h values. Here "bluer" means that one skylight color has a higher correlated color temperature than another, not necessarily that its colorimetric purity is larger. This holds true even though the antisolar horizon has a higher-contrast band of increased L_v near its horizon [*e.g.*, compare Figs. 6(a) and 6(b)], and this is sometimes interpreted visually as a whiter antisolar sky.

Finally, unlike my measurements made at sea level, Fig. 8's bluest skylight (see $\phi_{rel} = 180°$ curve at $h = 48.4°$) has a correlated color temperature approaching ∞ K, the theoretical limit for molecular single scattering [10,26]. Notice that the h where skylight is bluest differs markedly for the two ϕ_{rel}. This simple observation ultimately leads to an answer for the question posed above: blue skylight gets redder at high h because scattering by aerosols reddens *slightly* as our line of sight nears the sun.

Simulations with a 2nd-order scattering model developed for another paper in this issue [31] show that the spectra of Mie aerosol phase functions for haze-L polydispersions [22] produce net reddening by single scattering when $\Psi \sim 20°$–$135°$. Haze-M polydispersions produce similar results in the 2nd-order model, as do MODTRAN4 colorimetric simulations of aerosols' single-scattering effects on sky color. For $h_0 = 30°$, this Ψ interval corresponds to $h = 15°$–$90°$ at $\phi_{rel} = 180°$ and all h at $\phi_{rel} = 90°$. For all $\phi_{rel} = 90°$–$180°$, colorimetric analysis shows that the aerosol reddening is largest at the zenith and decreases toward the horizon, which is the trend measured in Fig. 8. If aerosols are removed from the 2nd-order model, then its high-h chromaticity hooks disappear. Thus the size, shape, and position of these hooks depend on the combined effects of (1) aerosol absorption and single scattering and (2) multiple scattering by both molecules and aerosols.

As we look upward along a clear-sky meridian, these two processes' relative weights change continuously. Desaturation from multiple scattering over large τ_{slant} predominates at low h, but this net reddening wanes (*i.e.*, skylight becomes bluer) as h increases and Ψ decreases from $h \sim 35°$–$55°$. Somewhere in this h interval, reddening due to spectral scattering by aerosols begins to dominate. Because τ_{slant} decreases relatively little at higher h, the minor spectral effects of aerosol single scattering persist here, and skylight reddens slightly toward the zenith. Yet this subtle interplay of single and multiple scattering is often a visual disappointment, since clear skylight typically only looks bluer as we near the zenith.

4. Measuring Haze Aerosols' Effects on Clear-sky Spectra and Colors

Thus far, we have studied the effects of haze on clear-sky colors by juxtaposing separate chromaticity curves for clear and turbid tropospheres. Alternatively, we can examine haze extinction's consequences directly by calculating an effective haze *spectral transfer function* TF_λ, which I define as

$$TF_\lambda = L_\lambda(\text{hazy}\,\Psi)/L_\lambda(\text{clear}\,\Psi), \tag{1}$$

or the ratio of spectral radiances in hazy and clear atmospheres at the same Ψ and h_0. This is a phenomenological function rather than one that analyzes any intermediate radiative-transfer details. However, it is related to (and seems to be as useful as) my earlier definition of effective overcast transmissivity at the earth's surface [32]. Thus Eq. (1) should be considered an illustrative tool rather than an analytical one, but when used with care it can provide some insights into the *combined* spectral and angular consequences of haze extinction.

Figure 9 shows the TF_λ at USNA for $\phi_{rel} = 90°$ on the hazy day of 31 August 2012 [$\tau_{aer}(380\ nm) = 0.2799$] versus the clear day of 10 September 2012 [$\tau_{aer}(380\ nm) = 0.08727$; see Fig. 1]. In Figs. 9 and 10, all underlying L_λ were measured with the Photo Research PR-650 spectroradiometer and are averaged over its 1° FOV. In both figures, each TF_λ spectrum is calculated from Eq. (1) as the *ratio* of spectral radiances on the two days at corresponding Ψ, h_0, and λ. Although the TF_λ values plotted in Figs. 9 and 10 depend on the particular choice of clear and hazy skies, this choice is not crucial so long as it is representative of the observing site, which is the case here. Note that unlike direct-beam transmissivity, $TF_\lambda > 1$ is entirely possible and simply means that the hazy sky is brighter than the clear sky at the given Ψ and λ.

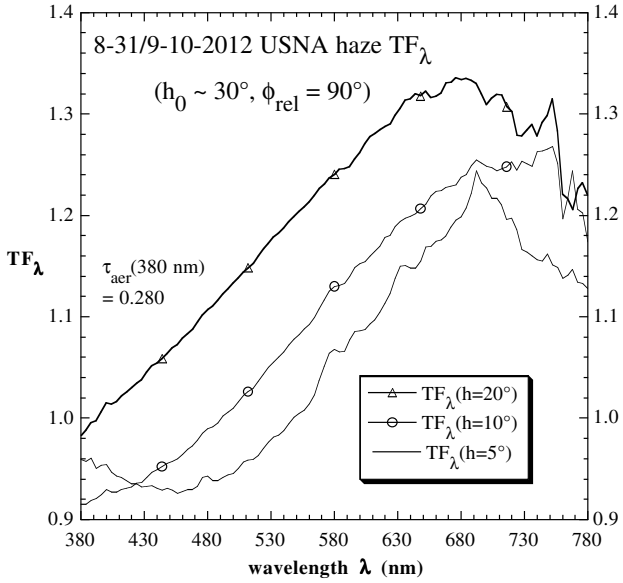

Fig. 9. Haze spectral transfer functions TF_λ for $h = 5°$, 10°, and 20° measured at USNA on 31 August 2012 and 10 September 2012 at $\phi_{rel} = 90°$. Each spectrum is calculated from Eq. (1) as the ratio of spectral radiances on the two days at corresponding Ψ, h_0, and λ.

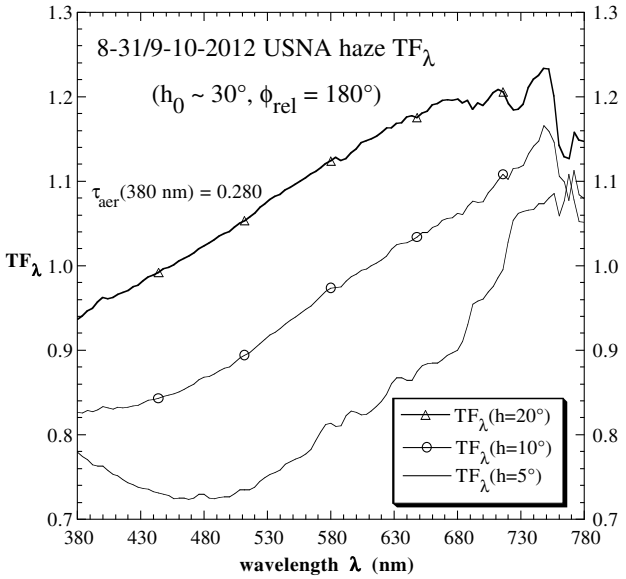

Fig. 10. Haze spectral transfer functions TF_λ for $h = 5°$, 10°, and 20° measured at USNA on 31 August 2012 and 10 September 2012 at $\phi_{rel} = 180°$.

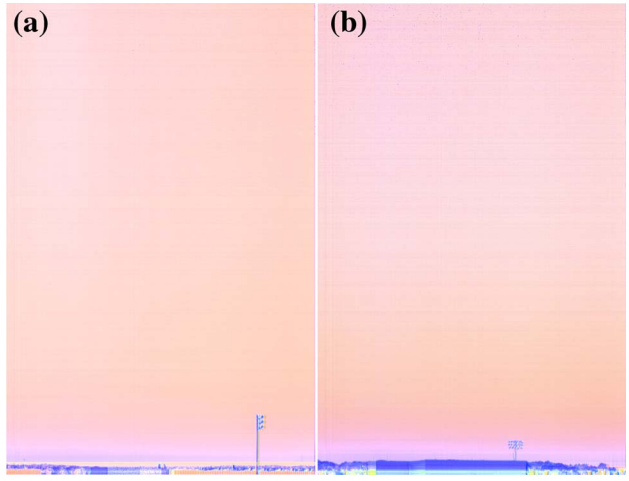

Fig. 11. False-color maps of TF_λ spectra measured at USNA for 13 September 2011 and 20 September 2010 at (a) $h_0 \sim 33.4°$, $\phi_{rel} = 270°$ and (b) $h_0 = 29.9°$, $\phi_{rel} \sim 180°$ at image center.

At $\phi_{rel} = 90°$ (or 270°), the following TF_λ trends are consistent in USNA clear skies: (1) a slight bluish bias at low h disappears by $h \sim 10°$, (2) with near-linear increases for $\lambda < 680$ nm at higher h, and (3) decreases for $\lambda > 680$ nm. The net result is that tropospheric haze often causes an *orangish* shift in clear-sky colors, except near the horizon where a purplish shift is more likely (see $h = 5°$ spectra in Figs. 9 and 10). The most significant differences in Fig. 10's antisolar sky are that Fig. 9's TF_λ local minima and maxima have shifted to longer wavelengths (to $\lambda \sim$ 480 nm and 750 nm, respectively). The net result is that haze-induced purplish and orangish color shifts tend to be more pronounced at $\phi_{rel} = 180°$ than at 90°, although much of this larger shift stems from the haze-free antisolar sky's more vivid blues. Strictly speaking, all such shifts also depend on h_0 and aerosol type, and they disappear (*i.e.*, $TF_\lambda \to 1$) as τ_{aer} decreases toward zero.

What might such haze-caused shifts in clear-sky colors actually look like? One answer appears in Fig. 11(a), a false-color map that plots Eq. (1)'s spectra pixel by pixel at equal Ψ for the hazy sky of 13 September 2011 [Fig. 2(b)] versus the clear sky of 20 September 2010 [Fig. 2(a)]. Figure 11(a) maps TF_λ near $\phi_{rel} = 90°$, while Fig. 11(b) does the same for TF_λ near $\phi_{rel} = 180°$. At matching pixels in each hazy:clear image pair, the TF_λ spectrum is used to calculate a u', v' chromaticity pair and a corresponding RGB ratio. Figure 11 plots these RGB triplets at maximum brightness, and so it only suggests each pixel's *spectral* distribution of TF_λ rather than its magnitude. For easier visualization, the transform from u', v' to RGB makes a completely uniform TF_λ spectrum equivalent to R = G = B (*i.e.*, the equal-energy spectrum is mapped into a white display color). Naturally, other false-color mappings are possible, but this one does address the question posed in Section 1: how to translate haze-induced shifts in clear-sky spectra directly into colors.

Figure 11's color maps trade the fine spectral details of Figs. 9 and 10 for much greater spatial detail. Although Fig. 11 uses spectral data from a different instrument (the Pika II imaging spectrometer) and from different days than those in Figs. 9 and 10, it tells much the same story about the typical effects of haze on USNA clear-sky spectra. First, the skies in both Figs. 11(a) and 11(b) have a distinct orangish to pinkish cast that becomes stronger near the horizon. Second, the overall color shift is redder in the antisolar sky of Fig. 11(b), unlike the case in Fig. 10 [compare slopes of the $TF_\lambda(h = 20°)$ curves in Figs. 9 and 10]. Third, immediately above the horizon are purplish color shifts like those seen at $h = 5°$ in Figs. 9 and 10, a shift that is stronger in Fig. 11(b)'s antisolar sky. These same angular trends appear in other USNA maps of TF_λ, suggesting that Fig. 11's haze color shifts are common here.

Figure 12 is a colorimetric version of Fig. 11. In it, TF_λ spectra at each h are averaged across a window 10° wide that is centered on $\phi_{rel} = 180°$ or 270° [see Fig. 2(b) for a color image of the latter sky]. As in Fig. 11, a spectrally uniform TF_λ is mapped into the equal-energy spectrum whose chromaticity is marked in Fig. 12. Now Fig. 11's TF_λ colors for the same hazy and clear skies (13 September 2011 and 20 September 2010, respectively), appear in Fig. 12 as chromaticity curves whose v' values increase as h increases near the horizon.

The gamut of these false colors is larger for $TF(\phi_{rel} = 180°)$, as indicated by (1) its chromaticity curve's larger span in Fig. 12 and (2) the more pronounced TF_λ colors in Fig. 11(b). Most of the change in Fig. 12's two TF_λ curves occurs within 5° of the horizon, reflecting the same trends as in Fig. 11. One TF_λ feature that is not evident in Fig. 11 is Fig. 12's pronounced pair of chromaticity hooks labeled "H" near $h = 40°$. Presumably, these are

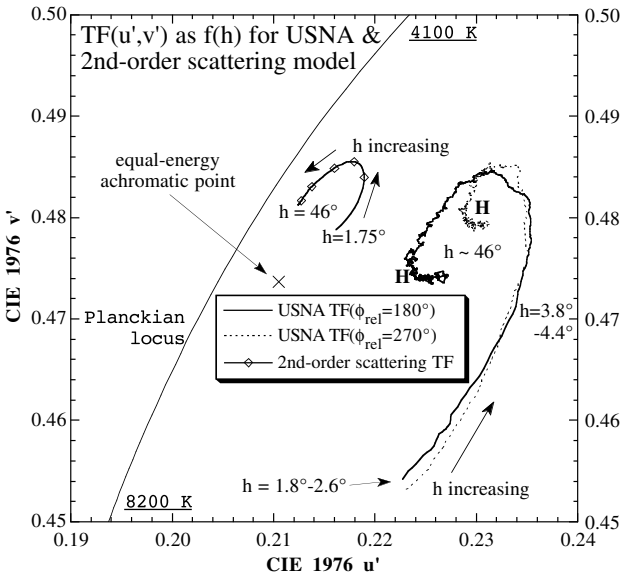

Fig. 12. Meridional TF_λ spectra measured at USNA for 13 September 2011 and 20 September 2010 at $\phi_{rel} = 180°$ and 270°, here plotted as the corresponding u', v' chromaticity curves.

the same hooks as seen in Figs. 3 and 5 for 13 September 2011, but now expanded by Eq. (1)'s spectral normalization. Also shown in Fig. 12 is a TF_λ chromaticity curve calculated by the 2nd-order scattering model [31] using Fig. 1's $\tau_{aer,\lambda}$ spectra. Like similar results from MODTRAN4, these simulated TF_λ have too small a colorimetric gamut, nor do they reproduce Fig. 12's measured chromaticity hooks. However, the 2nd-order model does duplicate the $TF_\lambda(\Psi)$'s essential behavior of haze color shifts that grow stronger and more purplish at low h. Despite its seeming simplicity, Eq. (1) nonetheless provides a quite useful criterion for testing the realism of radiative transfer models.

5. Conclusions

In principle, reproducing tropospheric haze colors and luminances at a particular time and place may seem to require highly detailed information on the micrometeorology and atmospheric single-scattering parameters of the site. Yet, in practice, one can start with fairly simple models and measurements: naked-eye observers at the earth's surface respond to skylight radiances that are integrated over broad spectral intervals and along long atmospheric paths. Thus we do not need to know haze extinction in minute spectral and spatial detail to explain what we see.

Yet we currently lack the most basic measurements of how haze aerosols *perceptibly* affect clear skylight. This paper provides a first round of those measurements at several sites over a period of three years. Among its findings are that haze aerosols at these sites:

1. desaturate the clear daytime sky's colors, but seldom by colorimetrically large amounts (see Table 1 and Figs. 3 and 4),
2. shift the loci of clear skylight chromaticities either parallel or perpendicular to the Planckian locus without much changing the original chromaticity curves' shapes (Fig. 5),
3. produce the chromaticity hooks that often occur at high h (see Figs. 3–5, 7, and 8),
4. redden skylight at all h but do so more strongly near the horizon (Figs. 9–12), and
5. cause a slight purplish shift in skylight just above the horizon (Figs. 9–12).

Thus far from being a mere colorimetric contaminant, haze proves to have surprisingly profound and wide-ranging visible effects on clear-sky colors. The measured properties of haze presented here are in fact perceptible, and they offer valuable new criteria for assessing the performance of radiative transfer simulations at visible wavelengths.

Raymond Lee was generously supported by United States National Science Foundation grant AGS-0914535 and by the United States Naval Academy's Departments of Mathematics and Physics. Opinions, findings, and conclusions or recommendations expressed in this paper are those of the author and do not necessarily reflect the views of the National Science Foundation. Thanks go to Jay Herman, Maria Tzortziou, and Gordon Labow of NASA's Goddard Space Flight Center for their efforts in establishing and maintaining its AERONET site and the $\tau_{aer,\lambda}$ data reproduced in Fig. 1.

References and Notes

1. J. E. Hansen, "Exact and approximate solutions for multiple scattering in cloudy and hazy planetary atmospheres," J. Atmos. Sci. **26**, 478–487 (1969). Hansen's calculations are for a near-infrared wavelength, but he notes that they could be extended to include the visible.
2. G. W. Kattawar, G. N. Plass, and S. J. Hitzfelder, "Multiple scattered radiation emerging from Rayleigh and continental haze layers. 1: Radiance, polarization, and neutral points," Appl. Opt. **15**, 632–647 (1976).
3. G. Zibordi and K. J. Voss, "Geometrical and spectral distribution of sky radiance: Comparison between simulations and field measurements," Remote Sens. Environ. **27**, 343–358 (1989).
4. S. Skouratov, "Vertical profiles of arctic haze aerosol in spring 1994 obtained by using spectrophotometric measurements," Atmos. Res. **44**, 113–124 (1997).
5. F. Zagury, "The color of the sky," Atmos. Clim. Sci. **2**, 510–517 (2012).
6. A still-valuable early work on both subjects is W. E. K. Middleton, *Vision through the Atmosphere* (University of Toronto, 1952), pp. 60–82, 145–174.
7. M. G. J. Minnaert, *Light and Color in the Outdoors* (Springer-Verlag, 1993), pp. 264–265, 288–291.
8. J. Gorraiz, H. Horvath, and G. Raimann, "Influence of small color differences on the contrast threshold: its application to atmospheric visibility," Appl. Opt. **25**, 2537–2545 (1986).
9. R. L. Lee, Jr., "Horizon brightness revisited: Measurements and a model of clear-sky radiances," Appl. Opt. **33**, 4620–4628, 4959 (1994).
10. R. L. Lee, Jr., "Twilight and daytime colors of the clear sky," Appl. Opt. **33**, 4629–4638, 4959 (1994).
11. R. C. Henry, S. Mahadev, S. Urquijo, and D. Chitwood, "Color perception through atmospheric haze," J. Opt. Soc. Am. A **17**, 831–835 (2000).

12. M. Gazzi, T. Georgiadis, and V. Vicentini, "Distant contrast measurements through fog and thick haze," Atmos. Environ. **35**, 5143–5149 (2001).
13. D. K. Lynch and S. Mazuk, "On the colors of distant objects," Appl. Opt. **44**, 5737–5745 (2005).
14. J. H. Taylor and H. W. Yates, "Atmospheric transmission in the infrared," J. Opt. Soc. Am. **47**, 223–226 (1957). Three of this paper's measured clear-sky transmission spectra include visible-wavelength intervals of 500–700 nm.
15. G. L. Knestrick and J. A. Curcio, "Measurements of spectral radiance of the horizon sky," Appl. Opt. **6**, 2105–2109 (1967).
16. R. C. Henry, "A field study of visual perception of complex natural targets through atmospheric haze by naïve observers," Atmos. Environ. **40**, 5251–5261 (2006).
17. J. Romero, R. Luzón-González, J. L. Nieves, and J. Hernández-Andrés, "Color changes in objects in natural scenes as a function of observation distance and weather conditions," Appl. Opt. **50**, F112–F120 (2011).
18. PR-650 spectroradiometer from Photo Research, Inc., 9731 Topanga Canyon Place, Chatsworth, California 91311 (http://www.photoresearch.com). According to Photo Research, at specified radiance levels, a properly calibrated PR-650 measures luminance and radiance accurate to within ±4%, has a spectral accuracy of ±2 nm, and its CIE 1931 colorimetric errors are $x < 0.001, y < 0.001$ for a 2856 K blackbody (CIE standard illuminant A).
19. Pika II hyperspectral imaging spectrometer from Resonon, Inc., 619 North Church Avenue, Bozeman, Montana 59715 (http://www.resonon.com). The system consists of a digital camera that has an internal diffraction grating and is coupled to a rotation stage controlled by a precision stepper motor and laptop computer. In this pushbroom system, the laptop acquires 640 different skylight spectra at each rotation stage position (*i.e.*, for each line of the resulting hyperspectral datacube). Each of the 640 pixels that make one scan line has its own spectral calibration, and the calibration procedure follows National Institute of Standards and Technology recommendations.
20. R. L. Lee, Jr., W. Meyer, and G. Hoeppe, "Atmospheric ozone and colors of the Antarctic twilight sky," Appl. Opt. **50**, F162–F171 (2011).
21. Sun photometer data and calculations of $\tau_{\mathrm{aer},\lambda}$ are acquired and archived by AERONET at http://aeronet.gsfc.nasa.gov. Fig. 1's data comes from the Goddard Space Flight Center in Greenbelt, Maryland and the Smithsonian Environmental Research Center in Edgewater, Maryland.
22. E. J. McCartney, *Optics of the Atmosphere: Scattering by Molecules and Particles* (Wiley, 1976), pp. 136–139.
23. C. F. Bohren and B. A. Albrecht, *Atmospheric Thermodynamics* (Oxford University, 1998), pp. 255–256.
24. B. I. Magi, P. V. Hobbs, T. W. Kirchstetter, T. Novakov, D. A. Hegg, S. Gao, J. Redemann, and B. Schmid, "Aerosol properties and chemical apportionment of aerosol optical depth at locations off the U. S. east coast in July and August 2001," J. Atmos. Sci. **62**, 919–933 (2005).
25. T. S. Glickman, ed., *Glossary of Meteorology*, 2nd ed. (American Meteorological Society, 2000), p. 363.
26. C. F. Bohren and A. B. Fraser, "Colors of the sky," Phys. Teach. **23**, 267–272 (1985).
27. C. F. Bohren, "Multiple scattering of light and some of its observable consequences," Am. J. Phys. **55**, 524–533 (1987).
28. For $h < 15°$, the near-infrared reflectance peak of trees and other vegetation along a given ϕ_{rel} is often seen in skylight spectra from $\lambda \sim 700$–900 nm. However, because surface reflections from 400 to 700 nm negligibly affect most clear skies for $h > 0.5°$, in this paper we can ignore surface reflectances along near-horizon paths and thus use relative (as opposed to absolute) azimuths.
29. The MacAdam JND is described in G. Wyszecki and W. S. Stiles, *Color Science: Concepts and Methods, Quantitative Data and Formulae*, 2nd ed. (Wiley, 1982), pp. 306–310.
30. C. F. Bohren and E. E. Clothiaux, *Fundamentals of Atmospheric Radiation* (Wiley-VCH, 2006), pp. 399–408.
31. R. L. Lee, Jr., "Measuring and modeling twilight's Belt of Venus," Appl. Opt. **54**, B194–B203 (2015).
32. R. L. Lee, Jr. and J. Hernández-Andrés, "Colors of the daytime overcast sky," Appl. Opt. **44**, 5712–5722 (2005).